SAND2018-4279C

6th European Conference on Computational Mechanics (ECCM 6)
7th European Conference on Computational Fluid Dynamics (ECFD 7)
11-15 June 2018, Glasgow, UK

MULTIFIDELITY UNCERTAINTY PROPAGATION FOR CARDIOVASCULAR HEMODYNAMICS

Daniele E. Schiavazzi[1], Casey M. Fleeter[2], Gianluca Geraci[3] and Alison L. Marsden[2]

[1] University of Notre Dame
153 Hurley Hall, Notre Dame, IN, 46556
dschiavazzi@nd.edu

[2] Stanford University
318 Campus Dr., Stanford, CA, 94305
cfleeter@stanford.edu
amarsden@stanford.edu

[3] SANDIA National Laboratories
PO BOX 5800, MS-1318, Albuquerque, NM 87185
ggeraci@sandia.gov

Key words: Cardiovascular modeling, Uncertainty quantification, Multilevel Monte Carlo sampling, Multifidelity Monte Carlo sampling

Abstract. Predictions from numerical hemodynamics are increasingly adopted and trusted in the diagnosis and treatment of cardiovascular disease. However, the predictive abilities of deterministic numerical models are limited due to the large number of possible sources of uncertainty including boundary conditions, vessel wall material properties, and patient specific model anatomy. Stochastic approaches have been proposed as a possible improvement, but are penalized by the large computational cost associated with repeated solutions of the underlying deterministic model. We propose a stochastic framework which leverages three cardiovascular model fidelities, i.e., three-, one- and zero-dimensional representations of cardiovascular blood flow. Specifically, we employ multilevel and multifidelity estimators from Sandia's open-source Dakota toolkit to reduce the variance in our estimated quantities of interest, while maintaining a reasonable computational cost. The performance of these estimators in terms of computational cost reductions is investigated for both global and local hemodynamic indicators.

1 INTRODUCTION

Hemodynamic models are increasingly used for disease diagnosis, treatment and for medical device design. A widespread adoption of such models in the clinical routine is hindered by the inability of deterministic modeling to quantify the variability in the predicted hemodynamic indicators of interest, and therefore to account for various sources

of uncertainty related, for example, to boundary conditions, segmented anatomy and material properties of living tissue. Stochastic modeling offers a solution to this problem at the expense of a substantial increase in the computational cost.

In this study, we leverage a cascade of model complexities arising naturally in the context of cardiovascular hemodynamics. Specifically, we discuss the use of estimators that are able to accurately capture the expected values of the quantities of interest while, at the same time, shifting the computational burden to the repeated solution of lightweight models of the physical system under study. To do so, we have developed automatic tools for the creation of lower fidelity cardiovascular models and have integrated these multiple fidelities with Sandia National Laboratories' Dakota toolkit [1] for UQ and optimization.

To frame the problem we are trying to solve in more formal terms, consider a complete probability space $(\Omega, \mathcal{F}, P)$ where Ω is a set of elementary events, $\mathcal{F}$ is a Borel σ-algebra of 2^Ω, and P is a probability measure with values in $[0,1]$ over events in $\mathcal{F}$. A vector of random variables $\boldsymbol{\xi} = (\xi_1, \xi_2, \ldots, \xi_d) \in \mathbb{R}^d$ with components $\xi_i : \Omega \to \Sigma_{\xi_i}$, $i = 1, \ldots, d$ of marginal distribution $\xi_i \sim \rho_i(\xi_i)$ and joint probability density $\rho(\boldsymbol{\xi})$, is used to parameterize model uncertainty. Finally, $\boldsymbol{x} \in D \subseteq \mathbb{R}^n$ and $t \in \mathbb{R}^+$ are the spatial and temporal variables, respectively. Specifically, we are interested in the statistical characterization of a generic quantity of interest (QoI) $Q = Q(\boldsymbol{x}, \boldsymbol{\xi}, t)$, e.g., through its m-th statistical moment $\mathbb{E}[Q^m]$ where, for a given realization $\boldsymbol{\xi}^{(i)}$ of the random inputs, Q is determined through the numerical solution of the incompressible Navier-Stokes equations on $D \subseteq \mathbb{R}^n$.

2 MULTIFIDELITY UNCERTAINTY PROPAGATION

Several challenges are typically faced when quantifying uncertainty in cardiovascular simulation outputs. First, several heterogeneous sources of uncertainty may affect the QoIs. Moreover, random inputs may be partially assimilated from clinical data, partially generated from spatio-temporal processes (e.g., random field representation of tissue constitutive properties) and partially assumed. Propagation of a large number of inputs poses significant challenges to approaches such as spectral stochastic expansion [2, 16], due to the fast increase of the computational complexity of tensor-products in high-dimensions. Additionally, three-dimensional simulations involve discrete representations with millions of degrees of freedom that are solved in parallel. Monte Carlo estimators [8] have, in this context, many desirable properties, i.e., are unbiased, can accommodate heterogeneous inputs and their rate of convergence does not depend on the underlying dimensionality. In particular, multilevel and multifidelity Monte Carlo estimators with reduced variance may be designed not to exceed a given computational budget [5, 4].

2.1 Multilevel and multifidelity Monte Carlo estimators

We introduce the *discretization level* M associated with the generic output Q, e.g., the number of degrees of freedom in the spatial or temporal discretization used to generate this output. The Monte Carlo estimator for the expected value of Q_M based on N realizations

is defined as

$$\mathbb{E}[Q_M] = \int_\Omega Q_M(\boldsymbol{x}, \boldsymbol{\xi}, t)\, \rho(\boldsymbol{\xi})\, \mathrm{d}\boldsymbol{\xi} \simeq \hat{Q}^{\mathrm{MC}}_{M,N} = \frac{1}{N}\sum_{i=1}^{N} Q_M^{(i)},\ \mathbb{V}[\hat{Q}^{\mathrm{MC}}_{M,N}] = \frac{1}{N}\mathbb{V}[Q_M], \quad (1)$$

where the i-th realization is denoted as $Q_M^{(i)} = Q_M(\boldsymbol{x}, \boldsymbol{\xi}^{(i)}, t)$. We also consider L (discretization or resolution) levels, i.e., $\{M_\ell : \ell = 0, \dots, L\}$, where $M_0 < M_1 < \cdots < M_L := M$. Using linearity of expectation and a telescoping sum, we re-write 1 as

$$\mathbb{E}[Q_M] = \mathbb{E}[Q_{M_0}] + \sum_{\ell=1}^{L} \mathbb{E}[Q_{M_\ell} - Q_{M_{\ell-1}}] = \sum_{\ell=0}^{L} \mathbb{E}[Y_\ell],\ \text{with } Y_\ell = Q_{M_\ell} - Q_{M_{\ell-1}}, \quad (2)$$

with $Q_{M_{-1}} = 0$. The *multilevel* Monte Carlo (MLMC) estimator for $\mathbb{E}[Q_M]$ is assembled from the estimators $\mathbb{E}[Y_\ell]$. At level ℓ, N_ℓ realizations are used to estimate Q_M^{ML} as

$$\hat{Q}^{\mathrm{ML}}_{M,N} = \sum_{\ell=0}^{L} \hat{Y}^{\mathrm{MC}}_{\ell,N_\ell} = \sum_{\ell=0}^{L} \frac{1}{N_\ell}\sum_{i=1}^{N_\ell} Y_\ell^{(i)},\ \mathbb{V}[\hat{Q}^{\mathrm{ML}}_{M,N}] = \sum_{\ell=0}^{L} \frac{1}{N_\ell}\mathbb{V}\left[Y_\ell\right]. \quad (3)$$

As before, the i-th realization $Y_\ell^{(i)}$ is evaluated at the i-th, $i = 1, \dots, N_\ell$, realization of the stochastic vector $\boldsymbol{\xi}$ with distribution $\rho(\boldsymbol{\xi})$. The advantages of the MLMC method come from the hierarchical nature of Y_ℓ, the difference in the QoI between successive resolutions. As $Q_M \to Q$ for $M \to \infty$, it follows that $Y_\ell \to 0$ as ℓ increases, and therefore the contribution to the overall variance from different resolution levels decreases with ℓ, shifting the computational burden to computationally cheaper coarser levels. The optimal sample allocation from each level can be determined by minimizing the computational cost of MLMC subject to a fixed target accuracy ϵ^2, evenly split between the variance and bias terms in the decomposition of the mean squared error. This leads to an optimal number of samples N_ℓ equal to

$$N_\ell = \frac{2}{\epsilon^2}\left(\sum_{k=0}^{L}\sqrt{\mathbb{V}[Y_k]\,\mathcal{C}_k}\right)\sqrt{\frac{\mathbb{V}[Y_\ell]}{\mathcal{C}_\ell}}. \quad (4)$$

where $\mathcal{C}_\ell$ is the computational cost of one evaluation of Y_ℓ. For an extensive review on MLMC estimators the reader can refer to [6].

Multifidelity approaches represent a *flavor* of the better known *control variate* (CV) variance reduction technique in Monte Carlo estimation. Two models are now defined, i.e., a low-fidelity (LF) and a high-fidelity (HF) model with an independent discretization level M. In this approach, the generic QoI Q_M^{HF} is replaced by $Q_M^{\mathrm{HF,CV}}$ which embeds a correction term based on the LF model [10, 9]

$$\hat{Q}^{\mathrm{HF,CV}}_{M,N} = \hat{Q}^{\mathrm{HF}}_{M,N} + \alpha\left(\hat{Q}^{\mathrm{LF}}_{M,N} - \mathbb{E}[Q^{\mathrm{LF}}_M]\right),\ \mathbb{V}[\hat{Q}^{\mathrm{HF,CV}}_{M,N}] = \mathbb{V}[\hat{Q}^{\mathrm{MC}}_{M,N}]\left(1 - \frac{r\,\rho^2}{r+1}\right), \quad (5)$$

with optimal regression coefficient α related to the Pearson's correlation coefficient between the LF and HF estimators, while r denotes the additional number of independent LF realizations $\Delta^{LF} = r\, N^{HF}$ needed to estimate $\mathbb{E}[Q_M^{LF}]$. For an extension to more than two fidelities, the reader may refer to [11].

Interestingly, we can combine the two ideas discussed above to further reduce the variance of our estimators, i.e., we consider one control variate for each (high-fidelity) resolution level ℓ or, equivalently, apply the multifidelity control variate idea to the Monte Carlo estimators associated to the difference Y_ℓ. Note that, unlike our derivation below, a different numbers of levels can be accommodated for high-fidelity and low-fidelity models. Starting from (2) we write a multilevel-multifidelity (MLMF) estimator as

$$\begin{aligned}\mathbb{E}[Q_M^{\mathrm{HF}}] = \mathbb{E}[Q_{M_0}^{\mathrm{HF}}] + \sum_{\ell=1}^{L} \mathbb{E}[Q_{M_\ell}^{\mathrm{HF}} - Q_{M_{\ell-1}}^{\mathrm{HF}}] = \sum_{\ell=0}^{L} \mathbb{E}[Y_{M_\ell}^{\mathrm{HF}}] \approx \sum_{\ell=0}^{L} \hat{Y}_{M_\ell,N_\ell^{\mathrm{HF}}}^{\mathrm{HF,MC}} \\ \approx \sum_{\ell=0}^{L} \left(\hat{Y}_{M_\ell,N_\ell^{\mathrm{HF}}}^{\mathrm{HF,MC}} + \alpha_\ell \left\{ \hat{Y}_{M_\ell,N_\ell^{\mathrm{HF}}}^{LF,MC} - \mathbb{E}[Y_{M_\ell}^{\mathrm{LF}}] \right\} \right).\end{aligned} \tag{6}$$

As before, we can determine the optimal sampling distribution (by level) N_ℓ^{HF} to compute $\hat{Y}_{M_\ell,N_\ell^{\mathrm{HF}}}^{\mathrm{HF,MC}}$ and $\hat{Y}_{M_\ell,N_\ell^{\mathrm{LF}}}^{\mathrm{LF,MC}}$ [5].

Finally, note that in addition to estimating quantities aside from the mean value for the quantity of interest, all the estimators discussed in the above sections can be further extended to handle multiple quantities of interest at once.

3 Modeling the cardiovascular system at multiple fidelities

High fidelity *three-dimensional* cardiovascular models are typically constructed from clinical image data of specific patients. In our workflow, these images are imported into the SimVascular open source platform [12] which provides a wide spectrum of algorithms for two- and three-dimensional segmentation, model creation, application of physiologic boundary conditions and includes a Streamline Upwind Petrov-Galerkin (SUPG) incompressible Navier-Stokes finite element solver. Hemodynamic simulations can be run with rigid or deformable walls, i.e., with or without accounting for the mutual interaction between fluid and structure. In this study, the coupled momentum method [3] is selected to model fluid-structure interaction (FSI).

One-dimensional hemodynamics are simulated through an in-house stabilized finite element solver [7, 14, 13, 15]. Blood is modeled as a Newtonian fluid, flowing along the axis of cylindrical branches; pressure is assumed to be constant over the entire vessel cross section, and a non-slip boundary condition is applied at the vessel lumen. The governing equations are obtained by integrating the incompressible Navier-Stokes equations over the cross section of a deformable cylindrical domain.

Finally, a *lumped parameter network representation* of blood flow is used as our lowest-fidelity model. This is a circuit layout formulated by hydrodynamic analogy in terms of flow rate (instead of electrical current) and pressure (instead of voltage), where each circuit element is associated to an algebraic or differential equation. These equations

are assembled in a system of ODEs which can be efficiently solved numerically with a 4th-order Runge-Kutta scheme. Resistors are used to represent viscous dissipation in vessels through friction at the endothelium, capacitors are used to represent vascular tissue compliance, and inductors are used to represent the inertia of blood. A Poiseuille flow assumption is used to determine the model parameters for these circuit elements.

4 Multilevel/Multifidelity Uncertainty Propagation

This section discusses uncertainty propagation on two hemodynamic models of the aorto-femoral and coronary circulation, respectively, under steady-state flow and resistance boundary conditions. A steady inflow waveform of 83.333 mL/s is prescribed at the aortic inlet for both models, consistent with the cardiac output of a healthy subject. The total outlet resistance is tuned to give a physiologic average pressure of 90 mmHg, again typical of an healthy subject, distributed proportionally to the outlet area (Murray's law, see, e.g., [17]). Thus, outlet resistance can be expressed as a vector $\mathbf{R} \in \mathbb{R}^9$ for the aorto-femoral model (9 outlets) and $\mathbf{R} \in \mathbb{R}^{10}$ for the coronary model (10 outlets).

After setting their reference values, the outlet resistances are considered as uncertain, leading to an input random vector $\boldsymbol{\xi} \sim \mathcal{U}[0.7 \cdot \mathbf{R}, 1.3 \cdot \mathbf{R}]$, i.e., with values drawn from uniform distributions of $\pm 30\%$ of the reference outlet resistance. Moreover, steady-state flows and pressures at the outlets are considered as our output quantities of interest, while wall shear stresses (WSS) are also considered for the coronary model.

The reduction in variance for these quantities of interest was compared for seven different estimators: "vanilla" Monte Carlo estimator (three-dimensional model only), two multifidelity estimators, three multilevel estimators, and one multilevel/multifidelity estimator, each discussed in Section 2. Schematics showing the relationship between the models in each method are shown in Figure 1, while a summary of the formulas for expected value and variance of our quantities of interest is provided in Table 1.

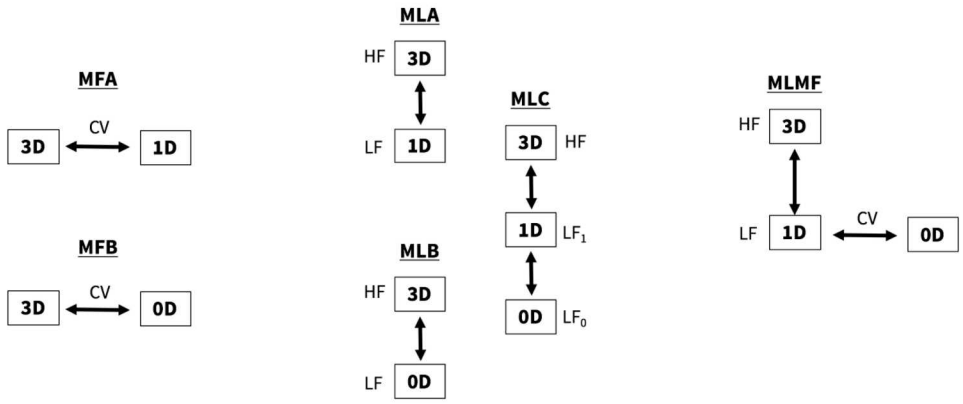

(a) Multifidelity. (b) Multilevel. (c) Multilevel/Multifidelity.

Figure 1: Schematics of multifidelity and multilevel UQ approaches.

Method	Expected Value	Estimator Variance
MC	$\hat{Q}^{\mathrm{MC}}_{N_{3D}} = \frac{1}{N_{3D}} \sum_{i=1}^{N_{3D}} Q^{(i)}$	$\frac{\mathbb{V}[Q]}{N_{3D}}$
MFA	$\hat{Q}^{MFA}_{N_{3D}} = \hat{Q}^{MC,3D}_{N_{3D}} + \alpha_{3D,1D} \left(\hat{Q}^{MC,1D}_{N_{3D}} - \mathbb{E}\left[Q^{MC,1D}_{N_{1D}} \right] \right)$	$\mathbb{V}\left[\hat{Q}^{\mathrm{MC}}_{N_{3D}} \right] \left(1 - \frac{r_{3D,1D}}{1 + r_{3D,1D}} \rho^2_{3D,1D} \right)$
MFB	$\hat{Q}^{MFA}_{N_{3D}} = \hat{Q}^{MC,3D}_{N_{3D}} + \alpha_{3D,0D} \left(\hat{Q}^{MC,0D}_{N_{3D}} - \mathbb{E}\left[Q^{MC,0D}_{N_{0D}} \right] \right)$	$\mathbb{V}\left[\hat{Q}^{\mathrm{MC}}_{N_{3D}} \right] \left(1 - \frac{r_{3D,0D}}{1 + r_{3D,0D}} \rho^2_{3D,0D} \right)$
MLA	$\hat{Q}^{MLA}_{N_{3D}} = \hat{Q}^{MC,1D}_{N_{1D}-N_{3D}} + \hat{Y}^{3D,1D}_{N_{3D}}$	$\frac{\mathbb{V}[Q^{1D}_{N_{1D}-N_{3D}}]}{N_{1D}-N_{3D}} + \frac{\mathbb{V}[Y^{3D,1D}_{N_{3D}}]}{N_{3D}}$
MLB	$\hat{Q}^{MLB}_{N_{3D}} = \hat{Q}^{MC,0D}_{N_{0D}-N_{3D}} + \hat{Y}^{3D,0D}_{N_{3D}}$	$\frac{\mathbb{V}[Q^{0D}_{N_{0D}-N_{3D}}]}{N_{0D}-N_{3D}} + \frac{\mathbb{V}[Y^{3D,0D}_{N_{3D}}]}{N_{3D}}$
MLC	$\hat{Q}^{MLC}_{N_{3D}} = \hat{Q}^{MC,0D}_{N_{0D}-N_{1D}} + \hat{Y}^{1D,0D}_{N_{1D}-N_{3D}} + \hat{Y}^{3D,1D}_{N_{3D}}$	$\frac{\mathbb{V}[Q^{0D}_{N_{0D}-N_{1D}}]}{N_{0D}-N_{1D}} + \frac{\mathbb{V}[Y^{1D,0D}_{N_{1D}-N_{3D}}]}{N_{1D}-N_{3D}} + \frac{\mathbb{V}[Y^{3D,1D}_{N_{3D}}]}{N_{3D}}$
MLMF	$\hat{Q}^{MLMF}_{N_{3D}} = \hat{Q}^{1D}_{N_{1D}-N_{3D}} + \alpha_{1D,0D} \left(\hat{Q}^{0D}_{N_{1D}-N_{3D}} - \hat{Q}^{0D}_{N_{0D}-N_{3D}} \right) + \hat{Y}^{3D,1D}_{N_{3D}}$	$\frac{\mathbb{V}[Q^{1D}_{N_{1D}-N_{3D}}]}{N_{1D}-N_{3D}} \left(1 - \frac{r_{1D,0D}}{1 + r_{1D,0D}} \rho^2_{r_{1D,0D}} \right) + \frac{\mathbb{V}[Y^{3D,1D}_{N_{3D}}]}{N_{3D}}$

Table 1: Expected values and variances of the Monte Carlo, Multifidelity, Multilevel and Multilevel/Multifidelity estimators with $Y^{3D,1D}_{N_{3D}} = \left(Q^{3D}_{N_{3D}} - Q^{1D}_{N_{3D}} \right), Y^{3D,0D}_{N_{3D}} = \left(Q^{3D}_{N_{3D}} - Q^{0D}_{N_{3D}} \right), Y^{1D,0D}_{N_{0D}-N_{1D}} = \left(Q^{1D}_{N_{0D}-N_{1D}} - Q^{0D}_{N_{0D}-N_{1D}} \right)$.

A fixed number of forward solutions associated with uniform realizations $\boldsymbol{\xi}^{(i)}$ were generated for this uncertainty propagation task. Specifically, 100 three-dimensional, 2 000 one-dimensional and 10 000 zero-dimensional simulations were used. Note how the first realizations are overlapping for the three model fidelities, i.e., the first 100 simulations were performed using the same random inputs for all fidelities, whereas the same 2 000 simulations were run for the one- and zero-dimensional models. All results were used in computing the estimators discussed above.

4.1 Aorto-Femoral model

The aorto-femoral model is a patient-specific model of a healthy abdominal aorta with iliac and femoral arteries, characterized by nine outlet branches. This model has no unusual/pathologic anatomical features such as stenosis or aneurysm, and has long, straight, quasi-cylindrical branches without large area differences at the outlets. The three model fidelities are illustrated in Figure 2. The relative cost of solving these models is reported in the footnote of Table 2. The difference in computational cost between 0D-1D and 1D-3D simulation time is very significant, i.e., several orders of magnitude. After examining the computational cost, outputs were compared to determine their degree of similarity/correlation across model fidelities. The distributions and ranges of the QoIs was found similar across fidelities which, together with a remarkable difference in computational cost, confirms a MLMF estimator to be particularly well-suited for this case.

Moreover, an idea of the reduction in variance with respect to the "vanilla" Monte Carlo estimator can be obtained by computing the Pearson's correlation coefficient. Figure 3 shows the square correlations for all QoIs, confirming an excellent potential for the MLMF

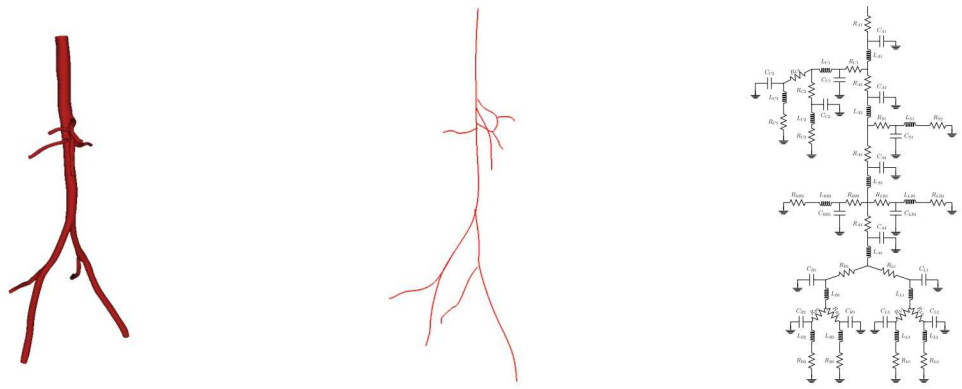

(a) 3D model. (b) 1D model. (c) 0D model.

Figure 2: Schematic view of the three model fidelities for the aorto-femoral model.

estimator to be associated with significant variance reduction with a small additional computational effort. The overall computational cost, in 3D simulation time units, for

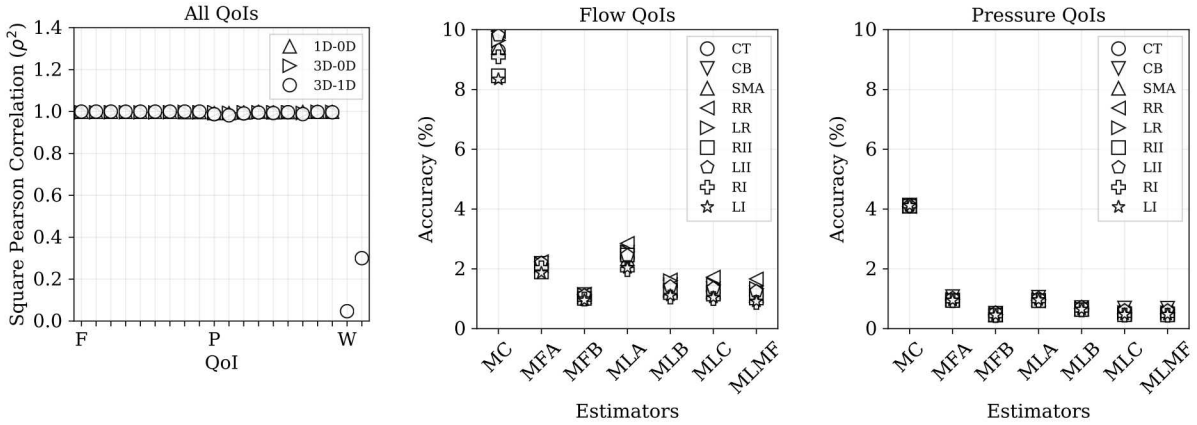

(a) Square correlations for all QoIs. F denotes flow, P pressure and W wall shear stress.

(b) Accuracy of flow QoIs for various estimators.

(c) Accuracy of pressure QoIs for various estimators.

Figure 3: Correlations and accuracy for QoI in aorto-femoral model.

the proposed multilevel/multifidelity estimators is shown in Table 2. Note that due to the cost difference across fidelities, several thousand 1D and 0D simulations contribute less than the cost of five additional 3D runs. Shaded rows on this table are used to highlight the methods using the same subset of the simulation results, and therefore having the same computational cost (though the associated variance reduction may vary).

A measure of the accuracy of output flow and pressure QoIs is computed in Figure 3 for each estimator. Accuracy is defined as the ratio of the $\pm 3\sigma$ confidence interval to

expected value,

$$\text{Accuracy}[Q] = \frac{6\sqrt{\mathbb{V}[Q]}}{\mathbb{E}[Q]} = \frac{(\mu + 3\sigma) - (\mu - 3\sigma)}{\mu} = \frac{6\,\sigma}{\mu}.$$

The mean flow at the right renal artery (RR in Figure 3b) appears to be the least accurate QoI. However, all multilevel and multifidelity estimators are associated to an accuracy lower than 3%, which is regarded as more than satisfactory in a clinical context. Also, pressure estimators are consistently more robust than flow estimators for this model. This is expected, as outlet pressures vary linearly as a function of outlet resistance while flow is distributed to the different branches inversely proportional to the associated resistance. The MFB estimator, i.e., the 3D-0D multifidelity estimator, provides the overall minimum variance for this model. This is expected due to the reduced geometrical complexity of the aorto-femoral model which justifies the high correlation between the QoIs of these two model fidelities. A reduced degree of correlation and less accurate estimators are instead expected for QoI such as local flow indicators or for pathological anatomies.

In Table 2, we extrapolated the number of total simulations required to obtain 1% accuracy in the mean flow at the right renal artery. The MFB estimator (together with the MFA estimator) requires a very limited number of 3D model solutions, compatible with a reasonable computational budget. The MFB estimator also requires three orders of magnitude fewer 3D model solutions than vanilla Monte Carlo, and approximately one order of magnitude fewer solutions than all multilevel estimators. These results are consistent with the high correlation of right renal flow among the models, as seen in Figure 3a, and the relatively small variance decay for this quantity of interest. Since the multilevel estimators rely on variance decay across levels for improved accuracy while the multifidelity estimators rely on high correlations, the latter require fewer model solutions to produce a target 1% accuracy, as expected.

	Pilot Run				Extrapolated cost			
Method	Effective Cost (*) (3D Simulations)	No. 3D Simulations	No. 1D Simulations	No. 0D Simulations	Effective Cost (3D Simulations)	No. 3D Simulations	No. 1D Simulations	No. 0D Simulations
MC	100	100	–	–	9 885	9 885	–	–
MFA	104.4192	100	2 000	–	56	21	15 681	–
MFB	100.1578	100	–	10 000	39	36	–	154 880
MLA	104.4192	100	2 000	–	305	212	41 990	–
MLB	100.1578	100	–	10 000	156	150	–	342 060
MLC	104.5754	100	2 000	9 900	165	156	1 324	351 940
MLMF	104.5754	100	2 000	9 900	165	156	1 249	362 590

(*) 3D model cost: 96hr (1); 1D model cost: 11.67min (2×10^{-3}); 0D model cost: 5sec (1.45×10^{-5}).

Table 2: Inter-fidelity computational cost comparison and extrapolation for aorto-femoral model.

4.2 Coronary model

The coronary model is generated from a healthy anatomy including aorta, left and right coronary arteries and ten coronary branches. No unusual/pathologic anatomical

feature, e.g., stenosis or aneurysm, is present in this model, similar to the aorto-femoral model discussed in the previous section. However, the fluid dynamics in the coronaries is associated with a higher degree of geometric complexity, due to large area differences between coronary and aortic inlets/outlets. The three model fidelities considered in this study are illustrated in Figure 4, with relative solution costs reported as a footnote in Table 3. For this coronary model, we have considered additional QoIs, such as several measures of wall shear stress (WSS), including its mean, minimum, and maximum values in both the whole model and individual branches and the percentage of lumen surface area on the model with WSS below a certain threshold. In the interest of brevity, we only discuss the results on the mean, minimum, and maximum WSS over the whole model.

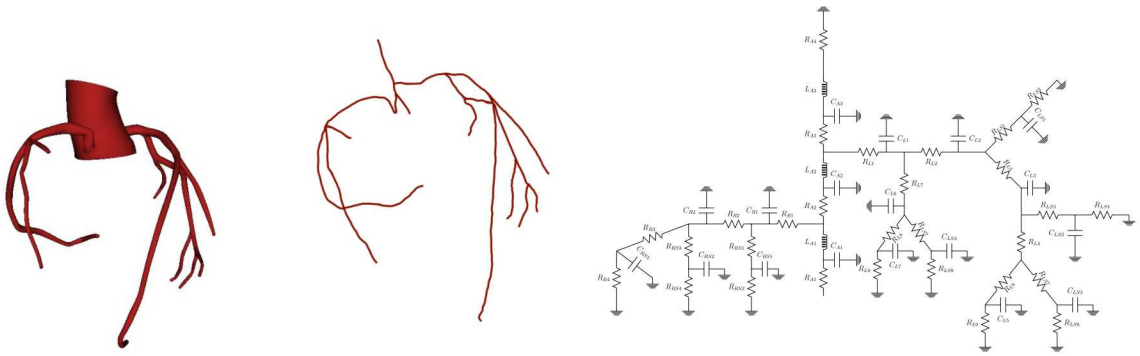

(a) 3D model (b) 1D model (c) 0D model

Figure 4: Schematic view of the three model fidelities for the coronary model.

Pearson's square correlations are still very close to one for the flows and pressures, as shown in Figure 5a. Conversely, the correlations for the three WSS-based quantities of interest (right of W in Figure 5a) vary significantly. The overall computational cost, in 3D simulation time units, for the proposed multilevel/multifidelity estimators is reported on the footnote in Table 3, while the resulting accuracies in the QoIs can be seen in Figure 5b and Figure 5c. All multilevel and multifidelity estimators of flows and pressures are associated to an accuracy lower than 9%, with pressure estimators consistently more robust than flow estimators for this model.

Finally, the total extrapolated number of simulations to obtain 1% accuracy for QoI *LC1Sub3* is reported in Table 3. The MFA estimator requires only seven 3D model simulations, much less than required for a similar extrapolation calculation in the aorta-femoral model. The MLC and MLMF estimators also require very limited numbers of 3D model simulations, showing these methods can be compatible with limited computational budgets. The MFA and MLA estimators both perform noticeably better than other multilvel estimators. These results are consistent with the high correlation shown in Figure 5a, and the relatively small associated variance decay.

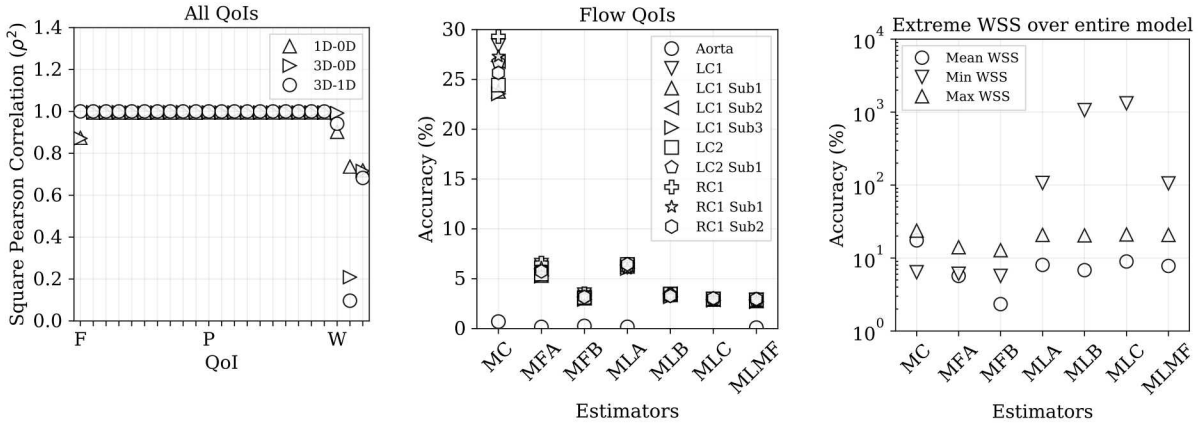

(a) Correlations for all QoIs. (b) Accuracy of flow QoIs. (c) Accuracy of WSS QoIs.

Figure 5: Correlations and accuracy in QoI for coronary model.

	Pilot Run				Extrapolated cost			
Method	Effective Cost (3D Simulations)	No. 3D Simulations	No. 1D Simulations	No. 0D Simulations	Effective Cost (3D Simulations)	No. 3D Simulations	No. 1D Simulations	No. 0D Simulations
MC	100	100	–	–	55 465	55 465	–	–
MFA	100.6410	100	2 000	–	30	7	71 640	–
MFB	100.1644	100	–	10 000	337	319	–	1 061 964
MLA	100.6410	100	2 000	–	92	47	140 351	–
MLB	100.1644	100	–	10 000	464	442	–	1 293 914
MLC	100.8037	100	2 000	9 900	42	32	9 862	395 160
MLMF	100.8037	100	2 000	9 900	40	31	6 886	405 863

(*) 3D model cost: 317hr (1); 1D model cost: 5.65min (3×10^{-4}); 0D model cost: 19sec (1.7×10^{-5}).

Table 3: Inter-fidelity computational cost comparisons for coronary model and extrapolated cost for 1% accuracy on the mean flow at left coronary (LC1 Sub3) artery.

5 Discussion and conclusion

In this exploratory study, we aimed to quantify the computational savings produced by MLMF estimators in cardiovascular modeling. In this context, the two uncertainty propagation test cases on aorto-femoral and coronary models serve to demonstrate the computational gain for possible future integration into our cardiovascular modeling pipeline.

Encouraging results were obtained. Specifically, we observed high correlations across pressure and flow QoIs for the two analyzed models, characterized by increasing geometrical complexity. These high correlations, together with a large range in computational cost suggested how a reasonable extrapolated computational budget is achievable with multifidelity estimators, as shown in Table 2 and Table 3. Substantial computational savings were also obtained by multilevel/multifidelity estimators compared to standard Monte Carlo, i.e., the number of 3D simulations needed to reach a target estimator variance was reduced by several orders of magnitude.

Future work will be devoted to include increasingly fine mesh discretizations, combining multiple levels and fidelities. This process was performed (not shown in this contribution)

during the development of the Dakota interface, using coarse, medium and fine meshes with both the three- and one-dimensional model fidelities (six models in total). Simulation realism will also be improved in future work. In this study, for example, we used simple resistors as boundary conditions, while RCR or closed-loop circuits are known to provide a more accurate physiological response. Also, pulsatile flow conditions will be considered together with local hemodynamic QoIs, averaged over one heart cycle. Finally, pathologic or diseased anatomies, e.g., abdominal aortic aneurysm or coronary artery stenosis will be investigated to improve our understanding of the performance of MLMF estimators for both healthy and pathologic patient-specific models.

Acknowledgments

This work was supported by a Center for Computing Research Summer Fellowship at Sandia National Laboratories (Casey Fleeter), an NIH R01EB018302-02 (P.I. Alison Marsden) and used computational resources from the Extreme Science and Engineering Discovery Environment (XSEDE), supported by National Science Foundation grant number ACI-1053575. We also acknowledge the open source SimVascular project at www.simvascular.org. Sandia National Laboratories is a multimission laboratory managed and operated by National Technology & Engineering Solutions of Sandia, LLC, a wholly owned subsidiary of Honeywell International Inc., for the U.S. Department of Energys National Nuclear Security Administration under contract DE-NA0003525. The views expressed in the article do not necessarily represent the views of the U.S. Department of Energy or the United States Government.

REFERENCES

[1] B. Adams, M. Ebeida, M. Eldred, G. Geraci, J. Jakeman, K. Maupin, J. Monschke, L. Swiler, J. Stephens, , D. Vigil, and T. Wildey, *Dakota, a multilevel parallel object-oriented framework for design optimization, parameter estimation, uncertainty quantification, and sensitivity analysis: Version 6.6 user's manual*, Sandia Technical Report SAND2014-4633, (2014).

[2] I. Babuška, F. Nobile, and R. Tempone, *A stochastic collocation method for elliptic partial differential equations with random input data*, SIAM Journal on Numerical Analysis, 45 (2007), pp. 1005–1034.

[3] A. Figueroa, I. Vignon-Clementel, K. Jansen, T. Hughes, and C. Taylor, *A coupled momentum method for modeling blood flow in three-dimensional deformable arteries*, Computer Methods in Applied Mechanics and Engineering, 195 (2006), pp. 5685–5706.

[4] G. Geraci, M. Eldred, and G. Iaccarino, *A multifidelity control variate approach for the multilevel monte carlo technique*, Center for Turbulance Research Annual Research Briefs, (2015).

[5] ——, *A multifidelity multilevel monte carlo method for uncertainty propagation in aerospace applications*, 19th AIAA Non-Deterministic Approaches Conference, (2017).

[6] M. Giles, *Multilevel monte carlo methods.*, Acta Numerica, 24 (2015), pp. 259–328.

[7] T. Hughes and J. Lubliner, *On the one-dimensional theory of blood flow in the larger vessels*, Mathematical Biosciences, 18 (1973), pp. 161–170.

[8] N. Metropolis and S. Ulam, *The Monte Carlo method*, Journal of the American Statistical Association, 44 (1949), pp. 335–341.

[9] L. Ng and K. Willcox, *Multifidelity approaches for optimization under uncertainty.*, International Journal for Numerical Methods in Engineering, 100 (2014), pp. 746–772.

[10] R. Pasupathy, M. Taaffe, B. W. Schmeiser, and W. Wang, *Control-variate estimation using estimated control means.*, IIE Transactions, 44 (2014), pp. 381–385.

[11] B. Peherstorfer, K. Willcox, and M. Gunzburger, *Optimal model management for multifidelity monte carlo estimation.*, SIAM Journal of Scientific Computing, 38 (2016), pp. A3163–A3194.

[12] A. Updegrove, N. Wilson, J. Merkow, H. Lan, A. Marsden, and S. Shadden, *SimVascular: An open source pipeline for cardiovascular simulation*, Annals of Biomedical Engineering, 45 (2016), pp. 525–541.

[13] I. Vignon, *A Coupled Multidomain Method for Computational Modeling of Blood Flow*, PhD thesis, Stanford University, 2006.

[14] I. Vignon and C. Taylor, *Outflow boundary conditions for one-dimensional finite element modeling of blood flow and pressure waves in arteries*, Wave Motion, 39 (2004), pp. 361–374.

[15] J. Wan, B. Steele, S. A. Spicer, S. Strohband, G. R. Feijo, T. J. Hughes, and C. A. Taylor, *A one-dimensional finite element method for simulation-based medical planning for cardiovascular disease*, Computer Methods in Biomechanics and Biomedical Engineering, 5 (2002), pp. 195–206.

[16] D. Xiu and G. Karniadakis, *The Wiener–Askey polynomial chaos for stochastic differential equations*, SIAM Journal on Scientific Computing, 24 (2002), pp. 619–644.

[17] Y. Zhou, G. Kassab, and S. Molloi, *On the design of the coronary arterial tree: a generalization of Murray's law*, Physics in Medicine and Biology, 44 (1999), p. 2929.